

Individual entanglements in a simulated polymer melt

E. Ben-Naim,¹ G. S. Grest,² T. A. Witten,¹ and A. R. C. Baljon³

¹*The James Franck Institute, The University of Chicago, Chicago Illinois 60637*

²*Corporate Research Science Laboratory, Exxon Research and Engineering Company, Annandale, New Jersey 08801*

³*Department of Physics and Astronomy, Johns Hopkins University, Baltimore Maryland 21218*

(Received 12 September 1995)

We examine entanglements using monomer contacts between pairs of chains in a Brownian-dynamics simulation of a polymer melt. A map of contact positions with respect to the contacting monomer numbers (i, j) shows clustering in small regions of (i, j) that persists in time, as expected for entanglements. Using the “space”-time correlation function of the aforementioned contacts, we show that a pair of entangled chains exhibits a qualitatively different behavior than a pair of distant chains when brought together. Quantitatively, about 50% of the contacts between entangled chains are persistent contacts not present in independently moving chains. In addition, we account for several observed scaling properties of the contact correlation function.

PACS number(s): 61.25.Hq, 83.10.Nn, 02.70.Ns

I. INTRODUCTION

Since the first theories of rubber elasticity, the notion of entanglement between polymer chains has been a central component [1]. Conceptually these entanglements are viewed as discrete constraints that limit the configurations of the chains, reduce their randomness, and thus contribute to the entropic stress in the rubber. These same entanglements are thought to be present in polymer melts. However, in a melt the entanglement constraints are not permanent. The diffusive reptationlike motions of each chain along its length permit chain ends to pass through a given entanglement and release the associated constraint [2]. In these theories entanglements are viewed as discrete objects, each making a comparable contribution to the elastic modulus.

A complementary view of entanglements is used in the tube model [1,2]. The tube model allows one to treat the fractional stress remaining as a function of time after a step strain. The magnitude of the modulus enters through the tube diameter, and there is no notion of discrete constraints. On the other hand, the notion of discrete constraints reappears when the model is refined [3,4]. For a complete theory it is necessary to account for the so-called tube-renewal or constraint-release effects. The tube consists of confining chains, and if an end of one of these confining chains crosses the tube, a constraint is released from the confined chain. As a result, an increment of stored free energy of order $k_B T \gamma^2$ is lost in a liquid under unit strain γ .

The double-reptation model of des Cloizeaux recognizes the implicit symmetry between the confining chain and the confined chain [6]. It treats all the elastic stress as arising from such constraints. This theory focuses on a particular entanglement constraint that involves two chains. Such an entanglement relaxes when either end of either chain passes through it. Tube disengagement and tube renewal are thereby treated as parts of a single phenomenon.

In all the above theories of polymer elasticity, the idea of discrete, spatially localized entanglements involving pairs of chains is present explicitly or implicitly. Yet only average properties, which ignore the individual nature of the entanglements, are discussed in these theories. In this study, we outline a strategy for identifying and characterizing *individual* entanglements in simulated polymer liquids. The strategy is based on the notion that an entanglement between two chains produces persistent contacts between them. Gao and Weiner [7] followed a similar path in a recent study. While they were unable to detect persisting contacts, they found that low mobility monomers tend to form clusters. We consider a sample of simulated chains, and our analysis of these chains provides suggestive qualitative and quantitative evidence of entanglements. We begin by describing the expected behavior of interchain contacts owing to entanglements. Next we describe a series of statistical measurements of these contacts using simulation results. Finally we assess these statistics in light of our expectations.

II. ENTANGLEMENTS AND PERSISTENT CONTACTS

We adopt a schematic model of a polymer chain widely used for simulations as well as for conceptual studies: a sequence of beads connected by anharmonic springs. The beads repel one another with a pairwise, short-range repulsion. We have simulated a liquid of such chains as described in the next section. In such simulations the beads move randomly under small stochastic forces as well as mechanical forces from the springs and from the bead repulsions. Such simulations have been used to give strong evidence for reptation [8,9]. Two beads may be said to be in contact if their separation is smaller than a predetermined threshold. Two long chains in a polymer melt that have one contact typically have many contacts. According to the conventional theory one expects two such chains to be *entangled* in a number of places

as well. These entanglements constrain the motion of the two chains in such a way as to increase the elastic modulus.

Entanglement constraints necessarily lead to attractive forces between chains. Furthermore, an entanglement confined to a certain segment of the chain implies contacts within that segment. The converse is not true since a contact at a given point does not imply an entanglement constraint there. Thus only a fraction of the contacts between two chains are associated with entanglements. The others are “incidental” contacts having nothing to do with entanglement constraints.

We expect incidental contacts and entanglement contacts to behave differently in time because entanglement constraints are long-lived. They are only released when a chain end passes through them. Accordingly, the forces and contacts that cause the constraint must be long-lived as well. Incidental contacts are not subject to such constraints and they may appear and disappear.

One way to visualize contacts between two chains is to form a “contact map.” This map is simply a matrix with one element for each pair of monomers (i, j) on the two chains in question. A contact between monomers i and j is indicated by $n(i, j) = 1$ in the matrix; all non-contacting elements are zero. Thus the contact map is a two-dimensional lattice of ones and zeros. We imagine the chains to be very long so that the matrix and the number of contacts are very large. The map then represents an irregular, diffuse cloud of contacts. As the system evolves in time, the cloud changes. Individual contacts appear and disappear, and similarly, a local cluster of contacts may translate, expand, contract, or change shape. A cluster consisting of incidental contacts can evaporate completely. On the other hand, if the contacts are caused by an entanglement, this is impossible since it would imply the removal of the constraint. Therefore, the entanglement contacts are persistent. These contacts may move but not disappear. They may only disappear (or appear) when the entanglement constraint does so. According to theory this happens when the entanglement goes to a chain end. Thus, entanglement contacts may only disappear when they have migrated to the boundaries of the contact map. Persistent contacts between two chains may also occur without entanglement. For example, the two sections of the chain may be held together by other chains, such as a third chain with a small loop through which the two examined chains pass. The resulting constraints may then be released if the loop is removed. This can happen if an end of the third chain passes through the constrained region.

The entanglements should be observable in various ways on the contact map. Qualitatively an entanglement is expected to appear as a localized cluster of contacts that maintains its average size and density as its position moves randomly over the map. If a sequence of maps is stacked to make a three-dimensional cloud of points, such an entanglement would appear as a loose, ropelike object persisting in the time direction. One may gain more quantitative information by analyzing the density of contacts $n(i, j, t)$. Since individual contacts have little significance in themselves, it is useful to average this density

over a few monomers in i and j . The resulting density \bar{n} is a smooth function of position and time. We expect this density field to have two contributions with qualitatively different dynamics. The entanglement-induced contacts decay significantly slower than the incidental contacts.

III. SIMULATION

The molecular dynamics simulation we used is identical to that used by Kremer and Grest [8,9] to study an equilibrium polymer melt. The melt is an ensemble of 200 chains, each containing $N = 350$ beads connected by springs. Individual monomers move according to the equation of motion

$$m\ddot{\mathbf{r}}_i = \nabla \sum_{i \neq j} U_{ij} - m\Gamma \dot{\mathbf{r}}_i + \mathbf{W}_i(t). \quad (1)$$

The potential U_{ij} contains two contributions. The first is a repulsive Lennard-Jones potential $U_{ij} = 4\epsilon[(\sigma/r_{ij})^{12} - (\sigma/r_{ij})^6 + 1/4]$ for $r_{ij} < 2^{1/6}\sigma$ and 0 otherwise between all monomers. The second is an anharmonic springlike interaction between bonded monomers [8]. Here Γ is the bead friction and $\mathbf{W}_i(t)$ is the random force acting on bead i . The strength of the random force is coupled to the bead friction by the fluctuation-dissipation theorem. The temperature $T = \epsilon/k_B$ and the density $\rho = N/V = 0.85\sigma^{-3}$. The model has an average bond length of $L = 0.97\sigma$ and a persistence length of $L_p = 1.32\sigma$. The equations are integrated with a time step $\Delta t = 0.013\tau_0$, where τ_0 is the standard of time in Lennard-Jones units, $\tau_0 = \sigma\sqrt{m/\epsilon}$. The temporal behavior of the melt is characterized by several time scales. For $t < \tau_e \cong 1.8 \times 10^3\tau_0$ the chains have yet to encounter the topological constraints, and the dynamics are well described by the Rouse model [5]. By comparing the mean-square displacement of a monomer in the Rouse relaxation regime with the Doi-Edwards theory [1], Kremer and Grest found that the entanglement length for this model is $N_e \cong 35$ [8]. Thus the chain length in the present simulation is approximately $10N_e$. The corresponding Rouse time scale for relaxation of chains along the tube, $\tau_R = \tau_e(N/N_e)^2 \cong 1.8 \times 10^5\tau_0$ is comparable with the duration of the simulation, viz., $2.2 \times 10^5\tau_0$. The time required for the initial entanglement constraints to relax completely, $\tau_d \sim N^3$, is beyond the simulation’s temporal range.

We recorded contacts between all pairs of chains in intervals of $10^4\Delta t$. We defined two monomers to be in contact when their separation $r_{ij} \leq 1.5\sigma$. We considered 20 pairs of chains that had a large (> 100) number of contacts at time $t = 0$. The behavior of contacts between the various pairs of chains followed the same pattern, and in the following we discuss contacts between two representative pairs of chains (chains 66 and 72, chains 1 and 96). These two pairs had an average number of contacts over the entire run of 180 and 100, respectively. We also considered chains that had no contacts during the simulation. In the following section we define phantom contacts between two distant chains. We will present data for two such typical pairs (chains 1 and 3, chains 1 and 4). Con-

tact maps are discussed in the next section, while in Sec. V a statistical analysis is carried for the real contacts as well as the phantom contacts. For convenience, we omit the chain labels and refer to the contacts as real contacts (66-72 and 1-96) or as phantom contacts (1-3 and 1-4).

IV. CONTACT MAPS

The anticipated behavior of the contacts is nicely demonstrated by a space-time plot of the contact map. As shown in Fig. 1(a), contacts between two monomers diffuse in space, disappear, and reappear. However, certain contacts strongly persist in space, forming “rope-like” structures centered around two monomers. Such structures might indicate that the two chains are subject to a topological constraint in the vicinity of these two monomers. To understand the role played by entanglements we construct “phantom contacts,” i.e., contacts

between chains that are not subject to entanglement constraints. We construct these phantom contacts by identifying two distant chains with no real contacts. We then define a phantom chain by translating a copy of the second chain so that its center of mass coincides with that of the first chain at time $t = 0$. The contacts between the phantom chain and the real chain are the phantom contacts. As the simulation proceeds, the contacts between the first chain and the translated second chain were identified, maintaining the same translation used initially. In this way, we construct a map of phantom contacts analogous to our map of real contacts. Since the phantom chain is far from the real chain, the phantom contacts cannot be influenced by interactions between the two chains, including entanglements. Yet according to the tube model, these contacts would evolve in the same way as in real chains, since in this model the chains are presumed to move independently whether they are near or far from each other.

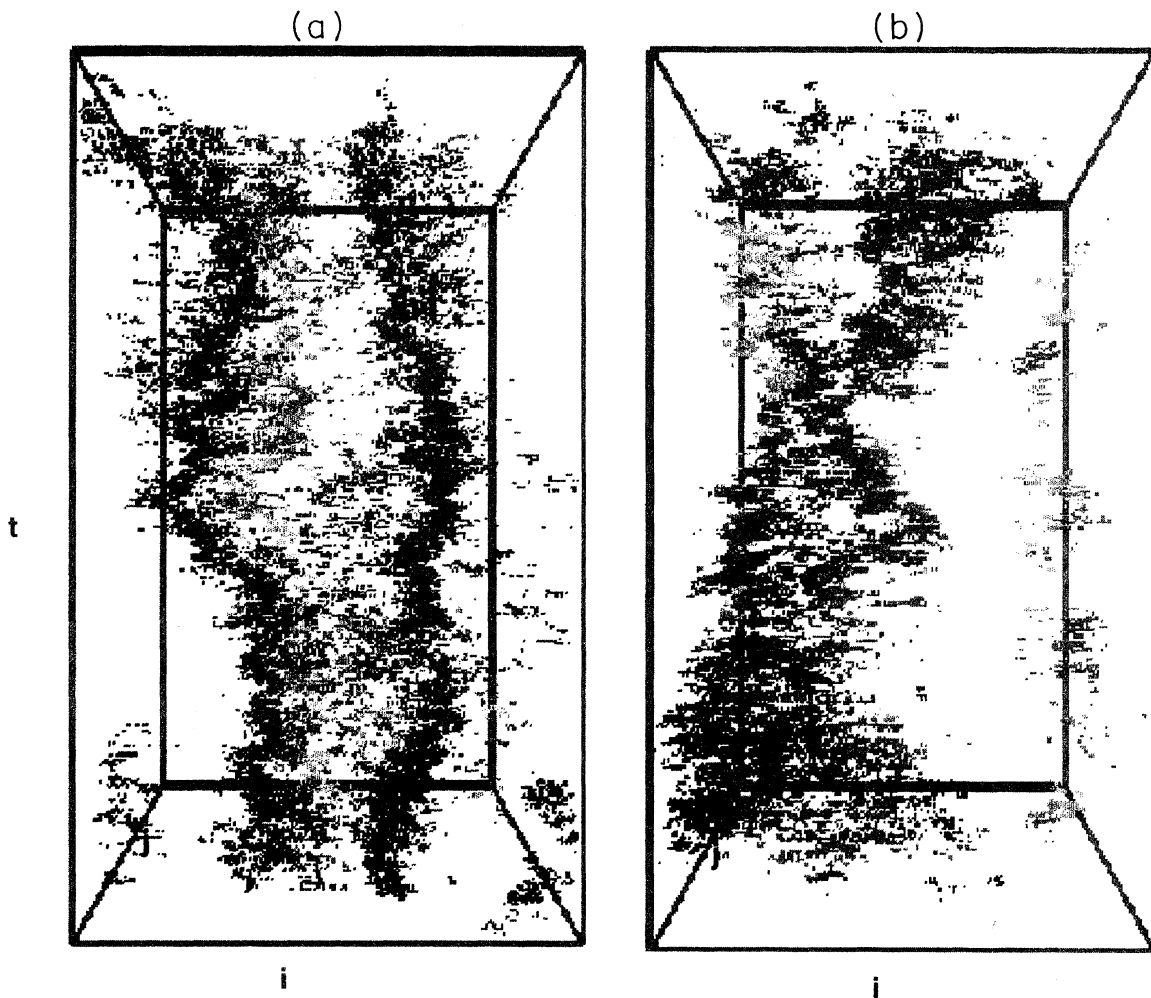


FIG. 1. Space-time representation of the contact map during the entire simulation. Shown are (a) real contacts (chains 66 and 72) and (b) phantom contacts (chains 1 and 4). The monomer index j is color-coded: foreground is blue, background is red.

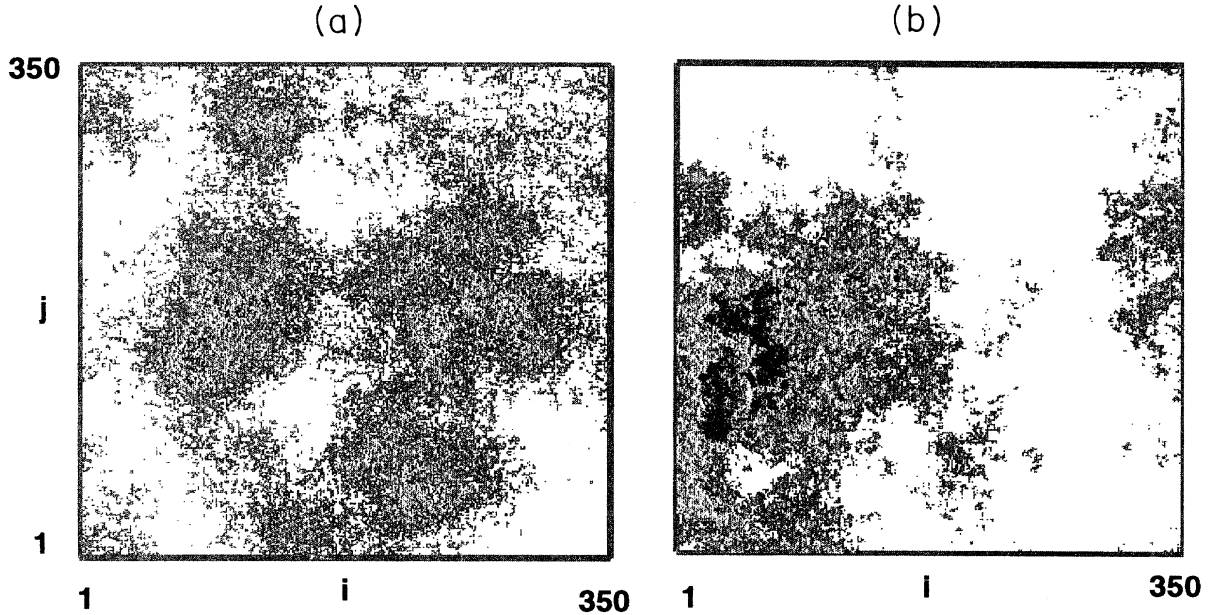


FIG. 2. Map of the total number of contacts between two monomers i and j during the simulation. Shown are (a) real contacts (chains 66 and 72) and (b) phantom contacts (chains 1 and 4). White indicates no contacts, red a small number of contacts, and blue many contacts.

Figure 1(b) nicely demonstrates the qualitative difference between the contact map of neighboring and distant chains. The phantom contact map consists of a large “cloud” of contacts, in contrast with the ropes that characterize real contact maps. This cloud suggests that phantom contacts have weaker spatiotemporal correlations. We also produced a map of all i - j contacts during the simulation, i.e., $\sum_t n(i, j, t)$. The contacts between the chains under consideration are confined to roughly three clusters that have not relaxed during the simulation [Fig. 2(a)]. Indeed, the number of clusters is consistent with the expected number of entanglements between two entangled chains, $\sqrt{N/N_e} \cong 3$. This estimate can be obtained by considering the overlap between two random walks of proper length in three dimensions. In comparison with real contacts, the phantom contact map appears more diffuse [Fig. 2(b)]. The above map suggests contacts between chains as an indicator of topological constraints, or, namely, entanglements.

V. STATISTICS OF CONTACTS

According to the contact map, real contacts between neighboring chains appear qualitatively different than phantom contacts between distant ones. In this section we present a quantitative tool for characterizing this difference. The primary feature of the contact map is the dominance of spatiotemporal correlations. Hence, we study the contact correlation function for both real and phantom contacts. Since the monomer index is equivalent to the curvilinear coordinate along a chain, and since

the dynamic behavior of this quantity is given in terms of simple scaling laws in time, we are able to predict the spatiotemporal properties of correlations between contacts. First, we detail the scaling predictions, and then we present numerical verifications of these scaling laws.

The contact correlation function provides a simple, direct way to compare the static and the dynamic properties of the chains. As mentioned previously, in each time frame τ , contacts between two chains, 1 and 2 for example, are given by the function $n(i, j, \tau)$. If monomers i of chain 1 and monomer j of chain 2 are in contact this function equals unity; otherwise, it vanishes. The contact correlation function, $g(x, y, t)$, is defined as

$$g(x, y, t) = N_{\text{tot}}^{-1} \sum_{\tau} \sum_{i, j} n(i, j, \tau) n(i + x, j + y, \tau + t), \quad (2)$$

where $N_{\text{tot}} = \sum_{\tau} \sum_{i, j} n(i, j, \tau)$ is the total number of contacts. With this definition $g(0, 0, 0) = 1$, and in general, $0 \leq g(x, y, t) \leq 1$. The correlation function has the following physical interpretation: $g(x, y, t)$ equals the conditional probability that monomers x and y are in contact at time t given that at time $t = 0$, monomers 0 on both chains were in contact.

Static properties are well described by the time independent correlation function $f(x, y) \equiv g(x, y, t = 0)$. Moreover, since chains in the melt have the global structure of a random walk, the asymptotic properties of this correlation function can be predicted by simple heuristic arguments. The quantity $f(x, y)$ is the conditional

probability that monomers x and y are in contact, given that both monomers 0 are in contact. Hence, one can view the two touching chains as a Gaussian ring of length $x + y$. The probability that such a chain forms a ring is simply $f(x, y) = P_{x+y}(r = 0)$ where $P_N(r) = (3/2\pi Na^2)^{3/2} \exp(-3r^2/2Na^2)$ is the end-to-end probability distribution function of a Gaussian chain with N beads and a is the monomer size. Hence, asymptotically one has

$$g(x, y, 0) \sim (x + y)^{-3/2}. \quad (3)$$

This correlation function has the advantage that it does not depend on the spacing between successive monomers.

The above argument should hold for real contacts as well as for phantom contacts. In Fig. 3 we show that both the real contacts and the phantom contacts follow the scaling relation of Eq. (3). Neighboring chains are subject to excluded volume effects, and thus they should experience an overall reduction in the number of contacts and in the static correlation function. Indeed, the static correlation function in Fig. 3 is larger for phantom contacts compared with real contacts.

To examine chain dynamics such as reptation, the time dependence of the correlation function is necessary. As for the static case, the leading long time behavior of the correlation function can be understood using simple arguments. One prediction of reptation theory is that in a melt the typical curvilinear displacement, $x(t)$, varies algebraically in time, $x(t) \sim t^{1/\alpha}$. The exponent α takes a series of values at increasing time scales [1]. Different time regimes are characterized by different α 's. For example, on the shortest time scale, the topological constraints have not been experienced by the chain. The

displacement is governed entirely by Rouse dynamics, $\alpha = 2$. Once the constraints are encountered, the dynamics are slowed down considerably, and as a result $\alpha = 4$. The crossover time between these two regimes is denoted by τ_e . The typical distance traveled in time t provides us with a natural time dependent length scale. Furthermore, we assume that the same scales dominate the contact correlation function. Hence, the time variable t is given in terms of the time scale associated with a curvilinear displacement x , x^α . For simplicity, we restrict our attention to the reduced correlation function, $g(x, x, t)$, whose expected scaling behavior is

$$g(x, x, t) \sim x^{-3/2} \Phi(z) \quad z = t/x^\alpha. \quad (4)$$

While in the short time limit, g reduces to the static correlation of Eq. (1), in the long time limit, $z \gg 1$, g is a function of t only. Consequently, the limiting behaviors of the scaling function $\Phi(z)$ are

$$\Phi(z)/\Phi(0) \simeq \begin{cases} 1 & z \ll 1 \\ Az^{-3/2\alpha} & z \gg 1. \end{cases} \quad (5)$$

For sufficiently long times, $t \gg x^\alpha$, one has $g(x, x, t) \sim t^{-3/2\alpha}$. In short, the complete contact correlation function is governed by a single exponent α .

According to the scaling prediction, $x^{3/2}g(x, x, t)$ at different times is a function of t/x^α only. We have verified this scaling hypothesis for both real and phantom contacts (see Fig. 4). However, the optimal exponent turned out to be $\alpha = 3$, in disagreement with the above theory. The reason for this discrepancy may be crossover effects, as the time regime where the contacts are observed is an intermediate one between the $\alpha = 2$ and $\alpha = 4$ time regimes. In fact, the temporal range we considered was $0 \leq \tau \leq 2.8 \times 10^3 \tau_0$, while the crossover

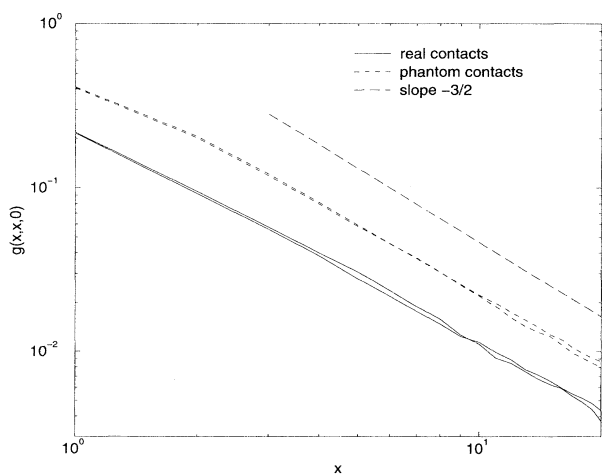


FIG. 3. Static correlation function, $g(x, x, 0)$ versus x . Real contacts (chains 66-72, 1-96, solid lines), as well as phantom contacts (chains 1-3, 1-4, dashed lines) follow the scaling law $g(x, x, 0) \sim x^{-3/2}$. The solid line with the slope $-3/2$ is shown for reference.

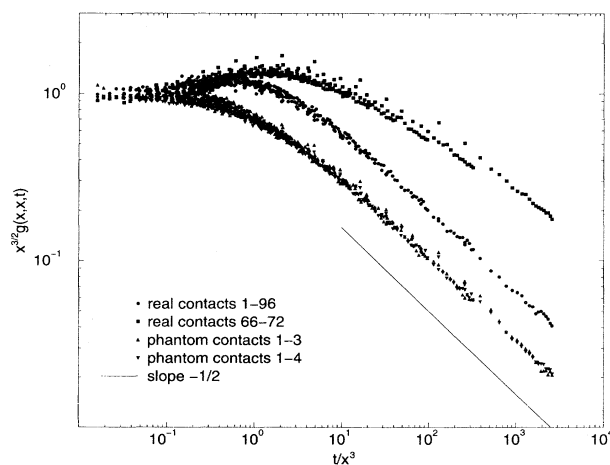


FIG. 4. Scaling of the the correlation function. The quantity $x^{3/2}g(x, x, t)$ plotted versus $z \equiv t/x^3$ for real contacts (66-72, squares; 1-96, circles) and phantom contacts (1-3, triangles; 1-4, inverted triangles). Following Eq. (5), the plots were vertically shifted, such that they approach unity as $z \rightarrow 0$. A line with the slope $-1/2$ is shown for reference.

between the two relevant regimes is $\tau_e \cong 1.8 \times 10^3 \tau_0$, as noted in Sec. III. It is expected that for longer times, the asymptotic value $\alpha = 4$ will be observed.

Figure 4 suggests that the scaling function $\Phi(z)$ is a different one for real contacts and for phantom contacts. Furthermore, a universal scaling function $\Phi(z)$ characterizes correlations between phantom contacts. This function decreases monotonically with increasing z . For real contacts, the scaling function exhibits a gentle maximum in the vicinity of $z = 1$. The strength of the maximum varied between roughly 1.3 and 1.5 for the real chains we examined (see Fig. 4). We use the strength of the maximum as a measure of the fraction of contacts arising due to entanglements. As a consistency check, we verified that contact maps of pairs with stronger maxima had more ropes compared with pairs that exhibited weaker maxima. From the definition of the scaling function [Eq. (4)], the position of this peak grows with time, $x \sim t^{1/\alpha}$. This observation suggests that persistent constraints are changing position along the chains, and as a result, the number of delayed contacts is increased. In other words, the longer one waits, the further the displacement of the constraint reaches.

This difference between real and phantom contacts can be equivalently illustrated by examining the time dependence of the correlation function with fixed monomer indices. In Fig. 5, $g(9,9,t)/g(9,9,0)$ is plotted versus t . While for phantom contacts g decreases monotonically in time, there is a peak in the real contact correlation function at $t > 0$.

In Fig. 4, the correlation function was rescaled by a constant factor such that it approaches unity when $z \rightarrow 0$. The asymptotic behavior of the scaling function is given by Eq. (5), $\Phi(z)/\Phi(0) \simeq Az^{-3/2\alpha}$, as $z \rightarrow \infty$. The asymptotic prefactor A is larger for real contacts than

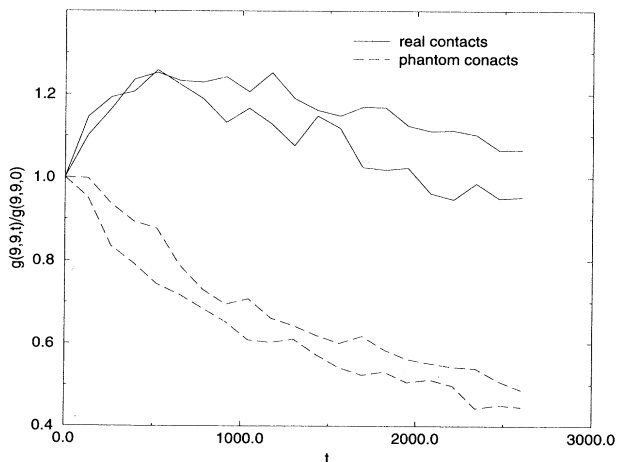


FIG. 5. Time dependence of the correlation function for a fixed monomer index. Shown is $g(9,9,t)/g(9,9,0)$ versus t for real contacts (66-72 and 1-96, solid lines) and phantom contacts (1-3 and 1-4, dashed lines).

for phantom contacts. The corresponding enhancement factor A strongly varied for the pairs of real chains we examined, and larger values of A were found for more localized contact maps. In other words, a fraction of the real contacts is persistent in time. We emphasize that all the chains we considered exhibited statistical properties similar to the above.

VI. DISCUSSION

The intriguing contact maps suggest that real contacts are qualitatively different from phantom contacts. These differences can be quantified using a statistical analysis of the maps. In this section we discuss the meaning of these differences and their relationship to entanglement.

We can describe the differences in terms of the properties of real or phantom contacts near a given contact. The overall density of contacts near a given contact is about half as large for real contacts as for phantom contacts. This is reflected in the smaller $g(x,x,0)$ for real contacts at all distances x . This difference is a simple consequence of the mutual avoidance of the real chains. Phantom monomer beads may intersect, but real beads can not. The intersecting configurations and their associated contacts are not available to the real chains, and thus fewer contacts are observed.

An opposing effect occurs when one considers *delayed* contacts near an arbitrary contact. For a given chemical separation x , we compare the number of contacts at a time delay t and separation x relative to the number of simultaneous contacts. For both real and phantom chains, the number of such contacts falls off progressively for long delays. Two initially contacting segments of length x eventually move away from each other, and their number of mutual contacts drops off. The number of delayed contacts is relatively greater for real chains than for phantom chains. Certain delayed contacts are more numerous than simultaneous contacts for a given separation x . They remain more numerous over delay times of the order required for a monomer to move a chemical distance x . The delayed contacts for real chains are typically 50% more numerous than for phantom chains. In other words, contacts near a given contact tend to persist longer in time for real chains than for phantom chains.

These extra persistent contacts may arise from entanglement between the two real chains. Indeed, persistence of contacts over time was the signature of entanglement anticipated in the Introduction. Our results suggest that roughly 50% of the contacts between two interpenetrating chains in a melt have motion that is dictated by entanglement constraints. For all 20 pairs of chains that we examined, this excess was between 30% and 50%, while there was no such fluctuation in delayed contacts for the phantom chains. This is a natural consequence of the discreteness of entanglements. We expect that some pairs of chains have more entanglements while others have fewer, and those pairs with fewer entanglements should have proportionally fewer persistent contacts.

By assuming that these persistent contacts arise from

entanglements, we can draw some implications about the entanglement contacts n_e and incidental contacts n_i postulated in the Introduction. The total number of contacts grows as the square root of the molecular weight; the number of entanglements between two chains expected in rubber-elasticity theory [1] grows at the same rate. Thus we expect n_e/n_i to be independent of molecular weight. If we identify the fractional excess of persistent contacts with n_e/n_i , we infer that $n_e \cong 0.5n_i$.

There is also the hint of a characteristic size x_0 in the contact correlations. The correlation function $g(x, t)$ shows a maximum as a function of t . This maximum is weak or absent for small x , and it reaches its asymptotic value for separations $x_0 \cong 10$. This characteristic separation may reflect a characteristic size for an entanglement.

Our analysis has led to suggestive evidence for entanglements. The persistent contacts we identified could well arise from other sources. For example local regions of two chains could be held together by other chains, thus resulting in persistent contacts. Nevertheless, the features we have identified appear consistent with the notion that the persistent contacts arise from entanglements between the two chains examined. The number of contacts seen in the contact maps or inferred from the decay of the correlation function is of the appropriate magnitude. The

size scale and relative number of the persistent contacts fits reasonably with the anticipated behavior for discrete, local entanglements, as well.

In conclusion, these results encourage the hope that entanglements may be identified as well-defined individual objects. If this identification could be made, it would lead to a deeper understanding and better control of polymer rheology. Our analysis can be used to distinguish entangled pairs of chains from unentangled ones. Additionally, the contact correlation function provides a natural probe of the dynamics of many chain systems and it will be interesting to use this technique to study the size and the mobility of individual entanglements. It might also prove useful to investigate properties of contacts in other many-chain systems.

ACKNOWLEDGMENTS

We thank J. Marko and A. Semenov for useful discussions. This work was supported in part by NSF under Grant No. 92-08527 and by the MRSEC Program of the National Science Foundation under Contract No. DMR-9400379. A.B. is supported by NSF Grant No. DMR-911004.

-
- [1] M. Doi and S. F. Edwards, *The Theory of Polymer Dynamics* (Clarendon Press, Oxford, 1986).
 [2] P.-G. de Gennes, *Scaling Concepts in Polymer Physics* (Cornell, Ithaca, 1979).
 [3] W. W. Graessley, *Adv. Polym. Sci.* **47**, 67 (1982).
 [4] D. S. Pearson, *Rubber Chem. Tech.* **60**, 439 (1987).
 [5] P. E. Rouse, *J. Chem. Phys.* **21**, 1273 (1953).
 [6] J. des Cloizeaux, *Europhys. Lett.* **5**, 437 (1988); Macro-

- molecules **23**, 3922 (1990).
 [7] J. Gao and J. H. Weiner (unpublished).
 [8] K. Kremer and G. S. Grest, *J. Chem. Phys.* **92**, 5057 (1990).
 [9] K. Kremer and G. S. Grest, in *Monte Carlo and Molecular Dynamics Simulations in Polymer Science*, edited by K. Binder (Clarendon Press, Oxford, 1995).

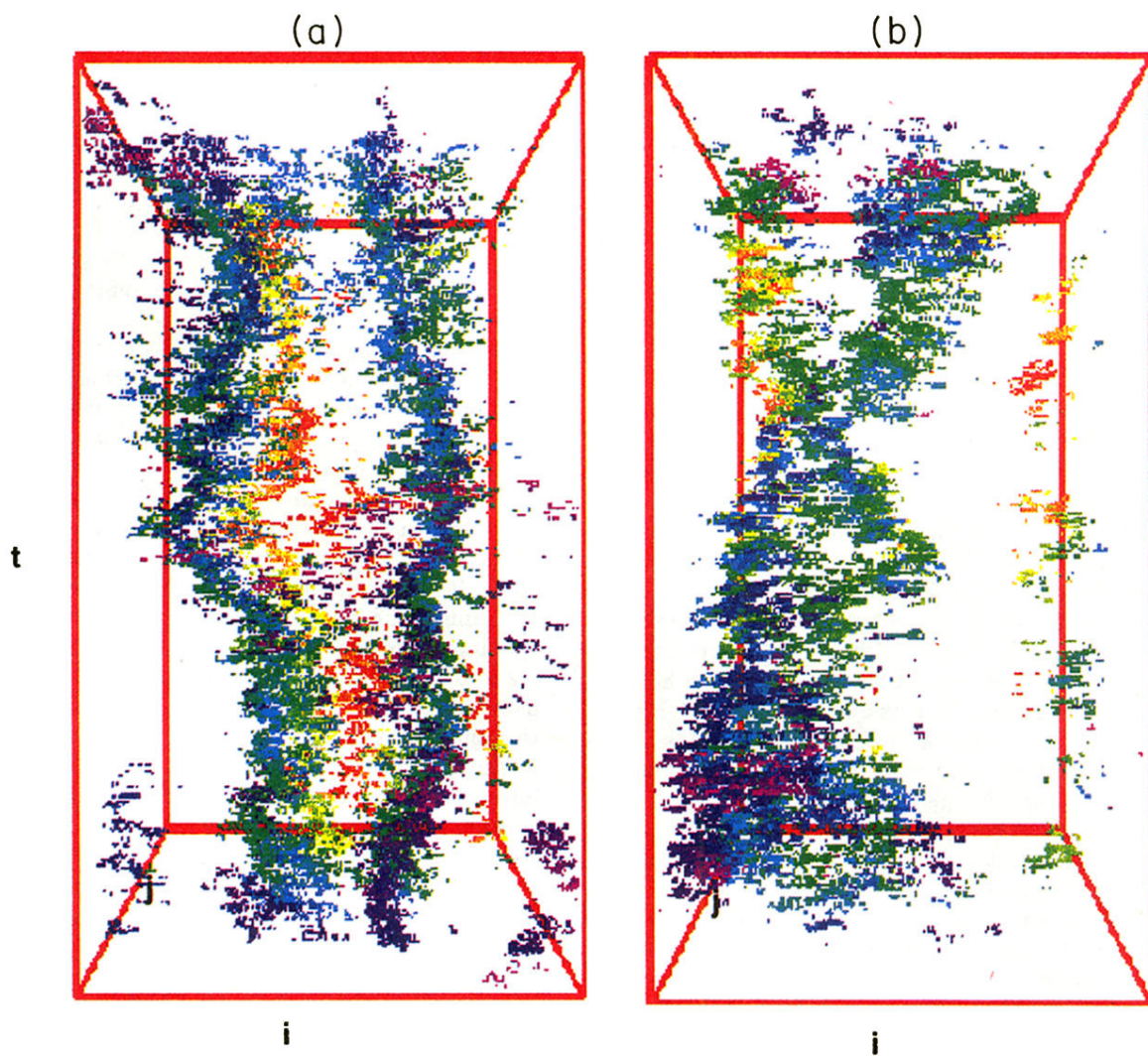


FIG. 1. Space-time representation of the contact map during the entire simulation. Shown are (a) real contacts (chains 66 and 72) and (b) phantom contacts (chains 1 and 4). The monomer index j is color-coded: foreground is blue, background is red.

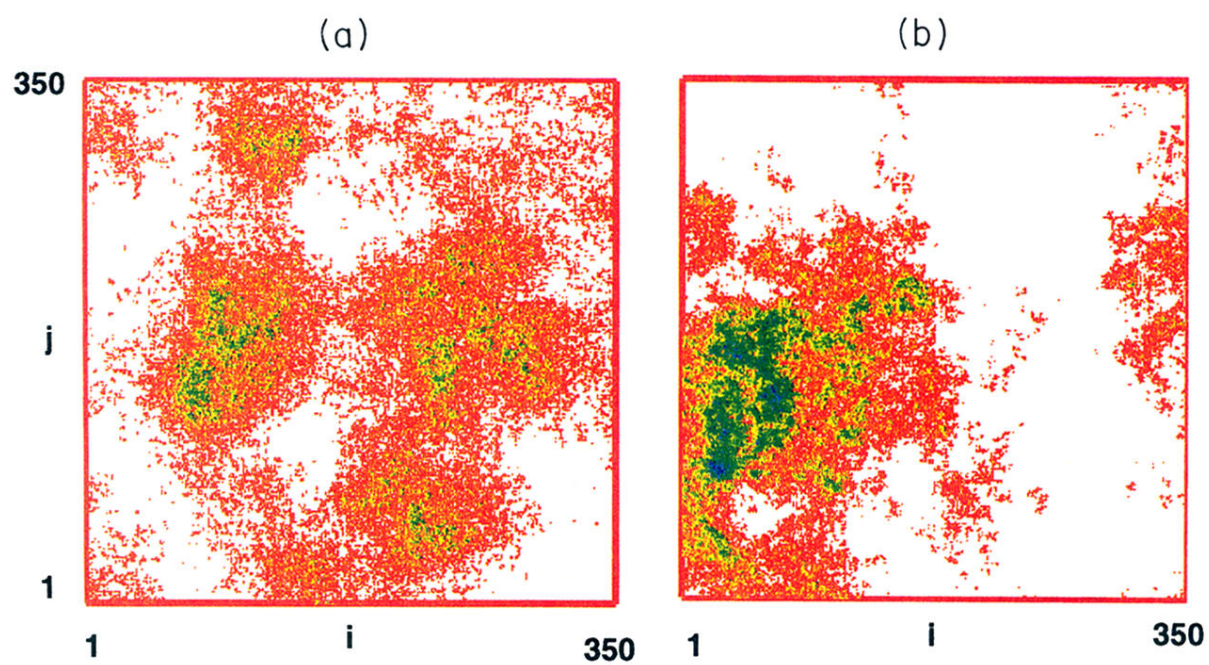


FIG. 2. Map of the total number of contacts between two monomers i and j during the simulation. Shown are (a) real contacts (chains 66 and 72) and (b) phantom contacts (chains 1 and 4). White indicates no contacts, red a small number of contacts, and blue many contacts.